Mansoura Engineering Journal ,(M.E.J) Vol. 20, No. 2 June 1995 M.88

Forced Convection Heat Transfer In a Cylindrical Porous Media exposed to Constant Wall Heat Flux

سريان الحمل الجبرى فى وسط مسامى دائرى معرض لفيض حرارى ثابت

M. S. El Kady

Power Mechanical Engineering Department
Mansoura University, Egypt

خلاصـــــه:

فى هذا البحث دراسة عدديه لانتقال الحرارة بالحمل الجبرى فى مجرى دائـرى مملوء بوسـط مسـامى معرض لفيض حرارى ثابت. يتكون النموذج من معادلة الطاقة بالإضافة إلـى معادلـة كميه الحركـة بصورتهـا العامة والتى تشتمل على التأثيرات اللادارسيه المختلفة مثل المسامية المتغيرة، القصور الذاتى للمـائع والاحتكـاك اللزج عند الحوائط، وقد استخدمت طريقه الفروق البسيطة فى الحل العددى. أجريت الدراسة على وسط مسـامى ذو حبيبات دائرية بأقطار $3 \le d \le 8$ mm ونسبه قطـر الحبيبـات الدائريـة الـى نصـف قطـر المجـرى الدائـرى $0.05 \le D \le 0.5$ وكذلك لانحدار فى الضغط B يصل الى 10^8. وقد أظهـرت التـأثيرات اللادارسيه تـأثيرا كبيرا على سلوك توزيع درجات الحرارة فى المجرى وعلى طول المدخل الحرارى وكذلك على معـدلات انتقـال الحرارة ممثله فى عدد نوسيلت على سطح المجرى ونتج عنها زيادة تقارب 21٪ فـى قيمـه عدد نوسيلت فـى نهايـة المدخل الحـرارى عـن ذلـك المسـتنتج مـن موديـل دارسـى الشـائع الاسـتخدام . وقـد أعطـت النتـائج ان المتغيرات المختلفة مثل قطر الكريات المكونة للوسط المسامى "d" ونسبه قطر الحبيبـات الكرويـة الـى نصـف قطر المجرى "D" ومعامل رينولدز للسريان "Re" وكذلك الانحدار فى الضغـط "B" لهـا تـأثيرا كبيـرا علـى توزيع درجات الحرارة وعلى طول المدخل الحرارى وكذلك على معدلات انتقال الحرارة. وتـم الحصـول علـى علاقات تصيغ اعتماد طول المدخل الحـرارى علـى المتغيـرات المختلفـة (d, D, B). وكذلك اعتمد طـول المدخل الحرارى اعتمادا مباشرا على عدد رينولدز للسريان، وأخـذت العلاقـة بينهمـا نفـس العلاقـة بيـن طـول المدخل الحرارى وعدد رينولدز فى حاله سريان المائع فى عدم وجود الوسط المسامى.

$$X_e \cong 0.1\ Re$$

للتأكد من صحة النتائج العدديـة أجريـت مقارنـات مـع النتـائج المذكـورة فـى بوليكـاكوس ورينكـن [11] ، كـايز وكراوفورد [26] وبيتشكوف [27] أظهرت تطابقا جيدا وأثبتت صحة هذا النموذج.

Abstract:

Forced convection heat flow in a cylindrical packed bed is examined numerically. The bed is filled with saturated spherical beads porous media and is exposed to a constant wall heat flux. Besides the energy equation, the generalized form of the momentum equation including the non-Darcian effects such as the variable porosity, flow inertia, and viscous friction is considered, and the finite difference method is used.

The results have been obtained numerically for sphere beads ($3 \leq d \leq 8$ mm diameter), ratio of the particle diameter to the pipe radius $0.05 \leq D \leq 0.5$, and nondimensional pressure gradient B up to 10^8. The non-Darcian effects have a significant influence on the behavior of the temperature, thermal entry length and Nusselt number across and at the channel wall. The channeling phenomenon near the walls enhanced the thermal communication between the fluid/solid matrix composite and the walls. This fact yielded an overall 21 percent increase in the value of the Nu in the fully developed region, compared to the value predicted when the Darcy model was used. The results gives complete information about the flow structure and heat transfer for the expressed ranges of parameters. Also, useful correlations reporting the dependence of the thermal entry length on the problem parameters (d, D, B) were reported. A direct dependence of the thermal entry length on Re exists and gives the same correlation that obtained for the pure fluid flow case:

$$X_e \equiv 0.1 \text{ Re}$$

To verify the numerical results a comparison have been done with the numerical results obtained by Poulikakos and Renken [11], Kays and Crawford [26] and Petukhov [27]. The comparison shows a very good agreement for the presented results and proves the validity of the model

1. Introduction

Fundamental studies related to thermal convection in porous media have increased significantly during recent years. This interest is due to the presence of porous media in diverse engineering applications including geothermal systems, building thermal insulation, enhanced recovery methods, nuclear waste disposal, packed bed chemical reactors, and solid matrix heat exchangers. Most of these studies address the problem of natural convection. The earlier investigations are based on the Darcy flow model and comprehensive reviews are provided by Combarnous and Bories [1], Catton [2] and El Kady [3]. In contrast to rocks, soil, sand and other media that do fall in this category, certain porous materials, such as foam metals and fibrous media, usually have high porosities. In these media, the boundary and inertia effects, not included in Darcy's model, may alter the flow and heat transfer characteristics. Therefore, lately, Non-Darcy effects on thermal convection in porous media have been considered by several investigators including Vafia and Tien [4], Poulikakos and Bejan [5], Kladias and Prasad [6], Lauriat and Prasad [7], and Ettefagh et. al. [8] among others.

The problem of forced convection in porous media is mostly relevant in flow through packed beds and the use of solid matrix heat exchangers. Koh and Colony [9] performed a simplifies analytical investigation of the performance of a heat exchanger containing a conductive porous matrix. However, the study was limited to very low permeabilities for which uniform velocity was assumed across the channel. In a study based on Brinkman-extended flow model, Kaviany [10] reported results for forced

convection in a porous channel bounded by isothermal parallel plates. Poulikakos and Renken [11] solved a similar problem but used a general flow model which included the effects of flow inertia, variable porosity, and Brinkman friction. Renken and Poulikakos [12] conducted an experimental study of boundary-layer forced convection from a flat isothermal plate in a packed bed of spheres. El Kady [13] investigated numerically the forced convection heat transfer and flow in an annular channel filled with porous media taking into consideration the non Darcian effects (flow inertia, variable porosity, and Brinkman friction). Cheng, et al. [14] analyzed the forced convection in the entrance region of a packed channel with asymmetric heating. Wang and Du [15] analyzed experimentally the forced convective heat transfer in a vertical annulus filled with porous media. Amiri and Vafia [16] simulate numerically the forced convective incompressible flow through porous media, and the associated transport processes. Kamiuto and Saitoh [17] examined numerically the fully developed forced-convection heat transfer in cylindrical packed beds with constant wall temperatures. Most of these studies relate to understanding the various physical phenomena which occur in existing porous-media-related thermal systems.

As an extension to these investigations, the present study performs a detailed numerical analysis of forced convection in a circular channel filled with spherical identical beads and exposed to a constant heat flux using the general flow model which includes the effects of flow inertia, variable porosity, and Brinkman friction. These non-Darcian effects, though not important in low-porosity media, are shown to be very significant in high-porosity media. A detailed information for these effects on the thermal entrance length, temperature variation in the channel cross section and the heat flow characteristics in the form of Nusselt number is reported.

2. Mathematical Formulation

A schematic for the physical configuration is shown in Fig. 1. It is assumed that the flow in the channel is steady hydrodynamically fully developed and a thermal entry region. The channel is a horizontal circular pipe filled with porous medium and is under uniform heat flux q_w on the outer surface. A saturated porous medium packed bed consisting of packed spheres is used to illustrate the results. It is assumed that the fluid and the solid matrix are in local thermal equilibrium. The thermophysical properties of the solid matrix and fluid such as the viscosity, thermal conductivity, effective thermal diffusivity are assumed to be constant.

Under these assumptions, the energy equation and the improved Darcy momentum equation including the viscous boundary friction and inertia effects can then be written.

$$u\ \partial T / \partial x = \alpha_e . 1/r\ \ \partial / \partial r (r\, \partial T / \partial r) \qquad (1)$$

$$\upsilon\, u / \gamma + A\, u^2 = -1/\rho .[\, \partial P / \partial x] + \upsilon / r . [\partial / \partial r (r\, \partial u / \partial r)] \qquad (2)$$

where u, P, T, ρ, α_e, υ are the velocity in the axial direction x, the pressure, the temperature, the fluid density, the effective thermal diffusivity and the fluid dynamic viscosity respectively. γ and A are the permeability and the inertia coefficient (Forschheimer function) of the porous medium and are given for the porous medium of identical spherical beads by

$$\gamma = d^2 \varepsilon^3 / [175 (1-\varepsilon)^2] \qquad (3)$$

$$A = 1.75 (1-\varepsilon) / [d \varepsilon^3] \qquad (4)$$

where d and ε are the spherical bead diameter and porosity, respectively. It is seen that the second term on the right hand side of equation (2) is an expression for the boundary viscous drag which was introduced first by Brinkman, the first and second terms of the left hand side are expressions for the Darcy frictional drag which is responsible for the porous structure and inertia drag. The present approach using equation (2) can be used from $\gamma \to 0$ (Darcian flow) to $\gamma \to \infty$ (Pure fluid flow).

Experimental observations of Benenati and Brosilow [18] indicate that the porosity in a randomly packed bed is functionally dependent on the distance from the boundary wall. A common practice is to consider an exponential decaying function to approximate the porosity variation. This can be expressed mathematically in the following form, which was used later by Vafia et.al [19], Poulikakos and Renken [11], and Mularidhar and Kulacki [20]:

$$\varepsilon = \varepsilon_e \ [1 + b \exp(- c [r_o - r] / d)] \qquad (5)$$

Where ε_e is the free stream porosity, and the empirical constants b and c are dependent on the particle diameter. The results will be illustrated by using spheres 3, 5 and 8 mm in diameter. The constants chosen to represent the variation of ε_e, b, and c are similar to that used by Benenati and Brosilow [18], Chandrasekhara and Vortmeyer [21] and the Author [13]. They are ε_e = 0.37, b=0.35, 0.43, 0.9 and c= 3, 3, 2 for d = 3, 5, 8 mm respectively.

At the outer radius there is a uniform heat flux q_w and no slip occurs. At the channel inlet, the fluid has a uniform velocity u_m and uniform temperature T_{in}, i.e. the following boundary conditions are applied:

$q = q_w$ and $u = 0$ at $r = r_o$

$T = T_{in}$, $u = u_m$ at the inlet section where $x = x_{in}$.

In order to nondimensionalize the governing equations (1) and (2), the following scalings are used:

$$U = u / u_m, \quad R = r / r_o, \quad D = d / r_o,$$

$$X = (x - x_{in}) / (r_o . Pr) \quad \text{and} \quad \theta = (T - T_{in}) / (q_w . r_o / \alpha_e)$$

The steady-state, dimensionless form of the governing equations (1) and (2) now become:

$$U\,\partial\theta/\partial X = [2/Re].1/R.[\partial/\partial R\,(R.\partial\theta/\partial R)] \qquad (6)$$

$$U + C_1.[Re/2].U^2 = B\,\Gamma.[2/Re] + \Gamma/R[\partial/\partial R\,(R.\partial U/\partial R)] \qquad (7)$$

where, $C_1 = 0.01\,D/(1-\varepsilon)$,

$\Gamma = \gamma/r_o^2 = D^2\varepsilon^3/[175\,(1-\varepsilon)^2]$,

$Re = 2\,u_m.r_o/\upsilon$, and

$B = -\partial P/\partial x.[r_o^3/\rho\,\upsilon^2]$

u_m is the averaged fluid velocity including the solid and fluid regions and B is the nondimensional pressure gradient.

The important heat transfer characteristics in a channel flow are indicated by the Nusselt number and the thermally entrance length which characterize the developing flow. Nusselt number at the wall can be derived in the dimensionless form as [11]:

$$Nu = \partial T/\partial r\big|_{r=r_o}.2\,[r_o/(T_w - T_m)] \qquad (8)$$

where the subscript w refers to the wall of the duct, T_m is the mean fluid temperature defined in a manner similar to that for classical fluid duct flows:

$$T_m = \left({}_0\int^{r_o} \rho\,u\,T\,dr\right)/\left[\rho\ {}_0\int^{r_o} u\,dr\right]$$

The thermal entrance length was defined as the distance between the entrance of the pipe and the point at which the mixed mean fluid temperature θ_m and the Nusselt number Nu became independent of the x-location. θ_m can be defined as:

$$\theta_m = (T_w - T)/(T_w - T_m)$$

3. Numerical Procedure

Because the problem is symmetrical with respect to the centerline, only the top half of the channel needs to be considered. An implicit finite difference method with variable grid in the X and R directions is employed. The R domain is discritized into 181 grid points to get an accurate resolution of the important near-wall region which is used to obtain the momentum equation finite difference form. A very fine grid size in the X direction near the channel inlet and coarser downstream is used. The grid size at the inlet is 0.0001 and increases gradually in the downstream direction. This is done to capture the steep changes in the temperature field near the entrance.

The momentum equation (7) was transformed into algebraic finite difference equations by integration, following the procedure developed by Patankar [22]. Since equation (7) pertains the forced convection, it can be solved independently to get the velocity field. Both the first and second order derivatives in the momentum equation (7) were discretized by using central difference formulas [23]. The Forschheimer nonlinear term is linearized by guessing initial valued of the velocity field at all the grid points, and the nonlinear term was written as the product of the unknown velocity and the guessed velocity. The difference algebraic momentum equation is solved using the Gauss-elimination method [22] to yield the velocity field. Utilizing the velocity distribution thus obtained, and after finite differencing the energy equation (6) using an implicit method, a system of tridiagonal algebraic equations for the nodal temperature at any given X position is obtained. The very powerful and convenient equation solver mainly the Thomas algorithm [23] is used to solve the system of equations beginning at X=0 and marching downstream. Once the temperature profile at each X position is known the local Nusselt number is determined from equations (8). When the local gradient of Nusselt number with respect to X is less than 0.001, a thermally fully developed flow is assumed and the entrance length is obtained.

4. Results and Discussion

On the basis of the present heat-transfer model, the effect of several system parameters such as d, D, B and Re on the entrance length, temperature profiles and heat transfer characteristics is examined. Also the effect of the non-Darcian terms in the momentum equation is examined on the temperature and Nusselt number. The present study covers the regions of $3 \leq d \leq 8$ mm, $0.05 \leq D \leq 0.5$, B $\leq 10^8$ and Re $\leq 10^4$.

4.1 Thermal Entrance Length

when the tube surface is fixed by imposing either a uniform temperature (T_w = const) or a uniform heat flux (q_w = const), the thermal entry length is the same [24]. From this phenomenonthe work of Poulikakos and Renken [11] for the case of (T_w = cons.) will be used here for the comparison and validation of the presented model. Fig. 2 shows the dependence of the thermal entrance length on the dimensionless pressure gradient B for the case of $d = 3$ mm and $D = 0.1$. The logarithmic scale shows the linear increase of the entrance length with the increase of the nondimensional pressure gradient B. It shows also the good agreement with the results of Poulikakos and Renken [11]. Fig. 3 shows the dependence of the thermal entrance length on the dimensionless pressure gradient B for the case of $d = 3$ mm and ratio of the particle diameter to the pipe radius $0.05 \leq D \leq 0.5$. Fig. 3 shows also the case of the pure fluid flow. The logarithmic scale presents the linear increase of the entrance length with the increase of the nondimensional pressure gradient B. It shows also the increase of the entrance length with the increase of the ratio D. Similar behavior to what was just described in conjunction with parameter B was observed when the dependence of the thermal entry length on the sphere-diameter-to channel radius ratio D figure 4 was investigated. With

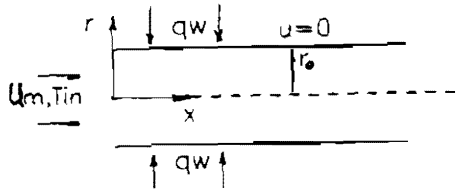

Fig. 1 Physical model, Coordinate system and boundaries

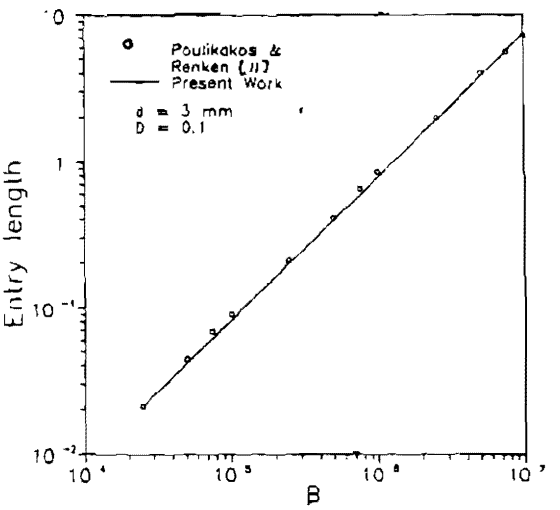

Fig. 2 Dependence of the thermal entrance length on the dimensionless pressure gradient B for d= 3 mm and D = 0.1,

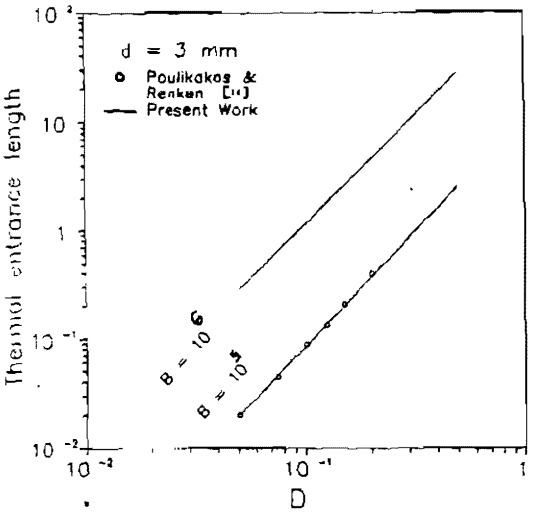

Fig. 3 Dependence of the thermal entrance length on D for different values of B and d = 3 mm

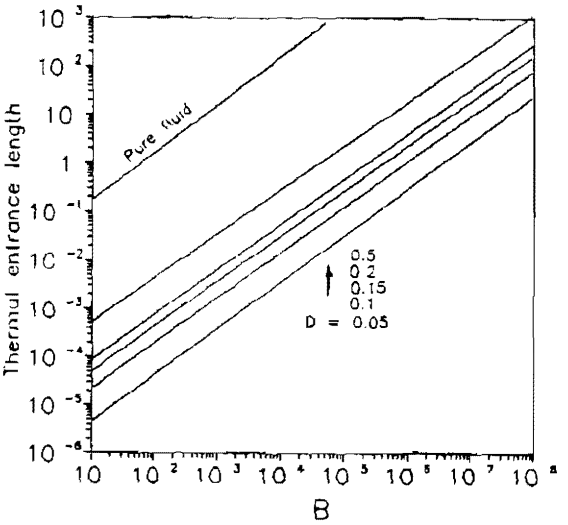

Fig. 4 Dependence of the thermal entrance length on B for d = 3 mm

the increase of the nondimensional pressure gradient B or the bead diameter d or the ratio D, Reynolds number increases [25]. This means the increase of the mean velocity of the flow which in turns decreases the thickness of the thermal boundary layer and leads to the increase of the thermal entry length. Fig. 4 shows also the comparison of the results for $B = 10^5$ with the results of the case (T_w = const). which was obtained by Poulikakos and Renken [11]. The results of this work show good agreement with the results of Poulikakos and Renken [11] and proves the validity of the model. The data points shown in Fig. 4 were correlated by the following equations:

$$X_e = 11\ D^2 \qquad \text{for } d = 3 \text{ mm},\ B = 10^5$$

$$X_e = 110\ D^2 \qquad \text{for } d = 3 \text{ mm},\ B = 10^6$$

Fig. 5 pertains a heat transfer result of engineering interest, namely, the dependence of the thermal entrance length X_e on Reynolds number. It is very interesting to notice that the various curves corresponding to the different cases expressed in figs. 2-4 besides the two cases of $d = 5$, 8 mm and $D = 0.1$, i.e. cases for different values of bead diameters and the ratio of bead diameter to the pipe radius, collapse on one curve coinciding with the case of pure fluid flow for laminar flow. The dependence on Re which is obtained here and was obtained by Kays et al. [26] for pure fluid flow gives by the existing variables definitions the following correlation:

$$X_e = 0.1\ \mathrm{Re}$$

This fact means that for constant Reynolds number the entrance length is independent on the bead diameter or the bead diameter to pipe radius ratio. By constant Reynolds number the mean velocity of the flow is the same, which gives the same thermal boundary layer and in turns the same entrance length. By increasing Reynolds number the flow becomes faster and the boundary layer thinner, which leads to higher values of the thermal entrance length.

4.2 Heat Transfer (Nusselt Number Variation)

Figs. 6 and 7 show the variation of the Nusselt number along the thermal entry region for a host of Reynolds number, $D = 0.1$ and $d = 3$, 8 mm. As it was expected, Nu decays rapidly as the thermal boundary layer develops, until the constant value associated with fully developed conditions is reached. Increasing Re which means faster flow yields to higher values of the Nusselt number throughout the thermal entry region.

Fig. 8 represents the Nusselt number variation in the thermal entry and the fully developed regions for different bead diameters 3, 5 and 8 mm, $D = 0.1$ with constant Reynolds number Re = 50. Nusselt numbers are, in principle, infinite at $X = 0$ and decay to their asymptotic (fully developed) values with increasing X. Higher values of Nusselt number exists along the entry and fully developed regions with the increase of the bead diameter d. Increasing d means more channeling effects (faster flow) near the boundary

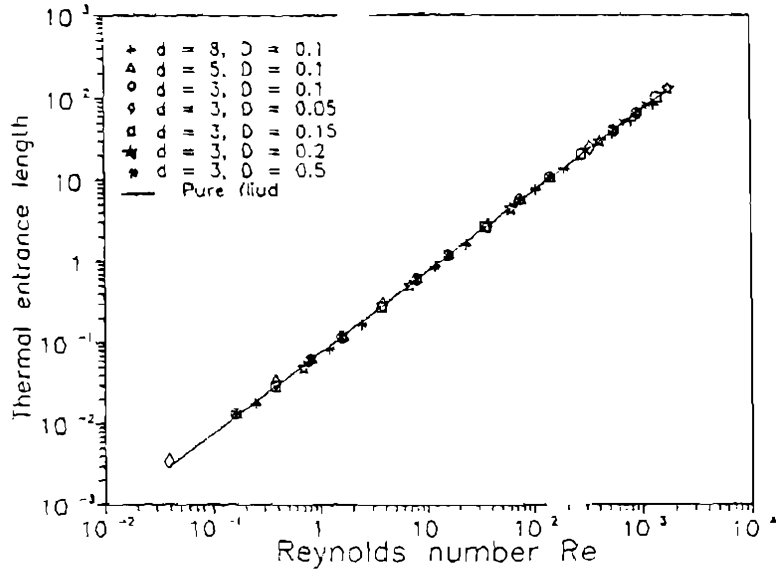

Fig. 5 the dependence of the thermal entrance length on Re for a host values of bead diameter d and bead diameter to channel radius D and for pure fluid flow

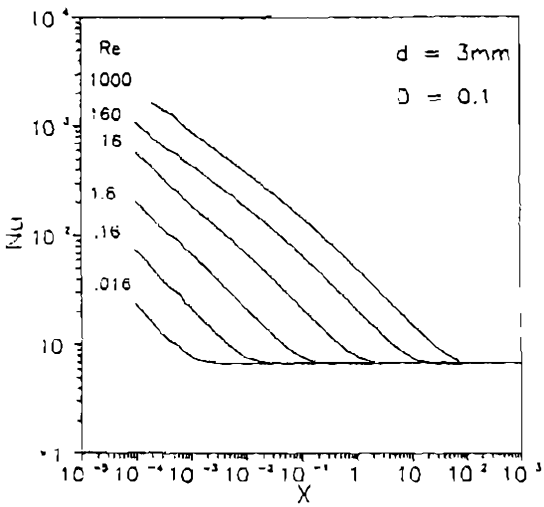

Fig. 6 the variation of Nu along the thermal entrance region for a host values of Re, $D = 0.1$ and $d = 3$ mm

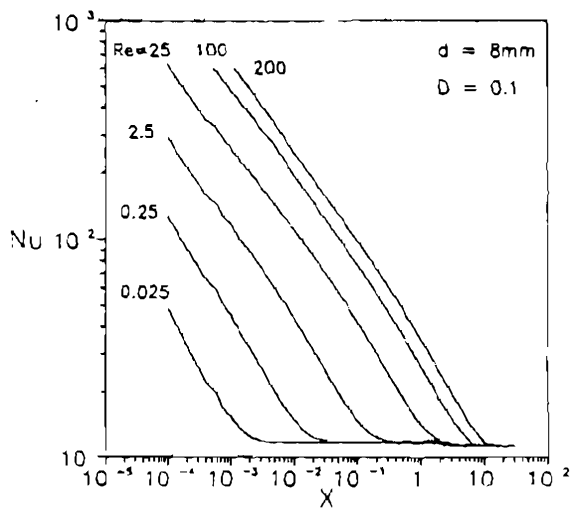

Fig. 7 the variation of Nu along the thermal entrance region for a host values of Re, $D = 0.1$ and $d = 8$ mm

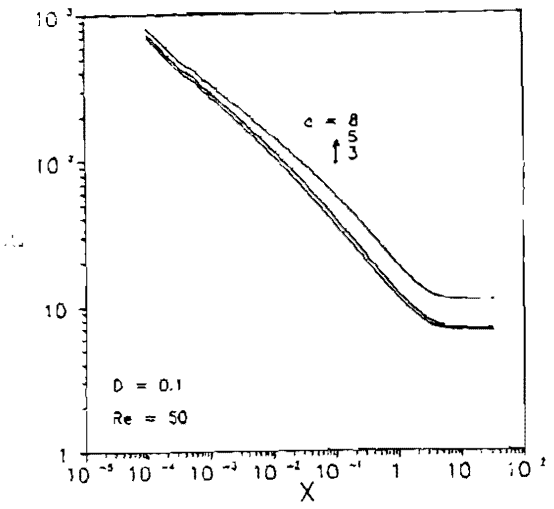

Fig. 8 Nu variation along the thermal entrance region for sphere diameters d = 3, 5 and 8 mm, Re = 50 and D = 0.1

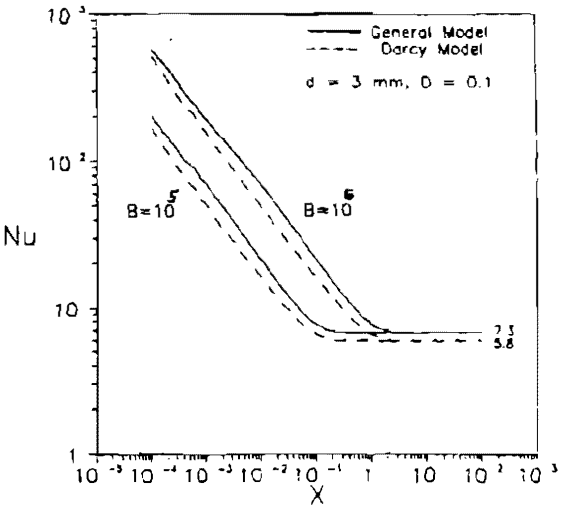

Fig. 9 Nu variation along the thermal entrance length for the dimensionless pressure gradients B = 10^5 and 10^6, d = 3 mm and D = 0.1

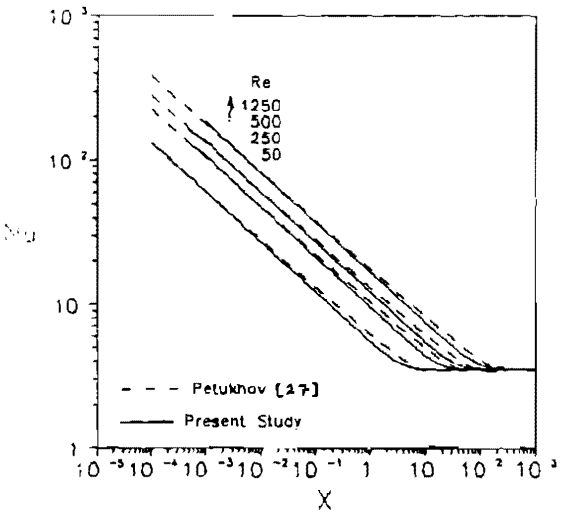

Fig. 10 Nu variation along the thermal entrance length for the case of pure fluid flow. A comparison with Petukhov [27].

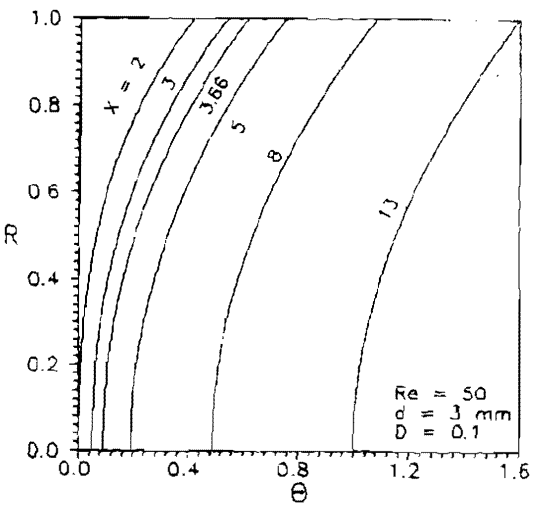

Fig. 11 Temperature distribution at several downstream locations for d = 3 mm, D = 0.1 and Re = 50

[25], which yields to relatively larger values of Nu throughout the thermal entry and fully developed regions.

Fig. 9 aims to identify the contribution of the non Darcian effects included in the discussed general model on the Nusselt number. The figure pertains the Nusselt number variation with the horizontal coordinate in the thermal entry region for the case of Darcy flow model where $\gamma \to 0$ and the general model for d = 3 mm, D = 0.1 and nondimensional pressure gradients B = 10^5 and 10^6. A noticeable increase of the value of Nu in the entry and fully developed regions taking into consideration the non-Darcian effects. The value of Nu in the fully developed region, including the effects of the Brinkman friction, flow inertia and variable porosity, is approximately 21 percent higher than the value predicted by the Darcy model.

To validate the existing heat transfer model, the pure fluid flow case is examined by assuming $\gamma \to \infty$ in the model and compared with the results of the correlation obtained by Petukhov [27] after rewriting it with the existing variables definitions:

$$Nu = 1.31\,[X/Re]^{-1/3} \cdot [1+2X/Re] \qquad (9)$$

Fig. 10 represents the Nu variation along the entrance region for the cases of pure fluid flow of Re = 50, 250, 500 and 1250 and the corresponding results obtained by equation (9). The comparison shows good agreement and validate the model.

4.3 Temperature variation

Fig. 11 shows the nondimensional temperature distribution across the pipe half width at several downstream locations X = 2, 3, 3.66, 5, 8, 13, where the entrance length X_e =3.66, bead diameter d = 3 mm, D = 0.1 and Re = 50. Typical temperature profiles are shown and characterized by a steep gradient at the wall owing to the effects of wall channeling.

Fig. 12 presents the variation of the temperature across the pipe half width at a location X= 3.66 for d = 3 mm, D = 0.1 and different values of Re = 50, 100, 500. With the increase of Re the mass flow rate increases which decreases the nondimensional temperature θ (the difference between the local temperature and the inlet temperature). Also, the increase of Re, i.e. faster flow, leads to thinner thermal boundary layer which yields smaller temperature difference between the boundary and the core of the flow.

Fig 13 pertains the variation of the nondimensional temperature θ across the pipe half width for different bead diameter d = 3, 5, 8 for constant Re = 50. Fig. 13 shows that with the increase of the bead diameter d the nondimensional temperature θ near the boundary, i.e. at the thermal boundary layer, decreases while it increases in the core of

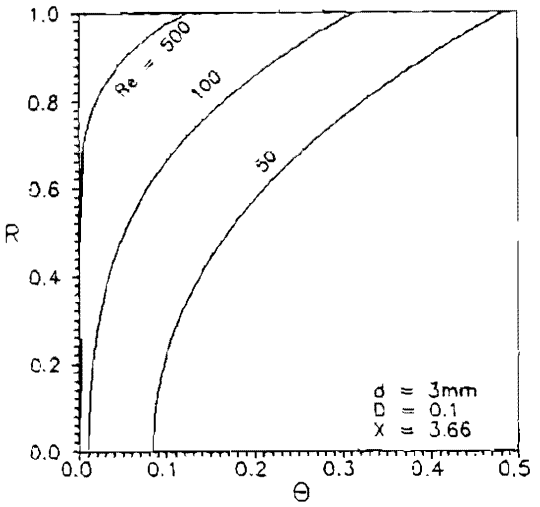

Fig. 12 Temperature distribution at X_e = 3.66 for d = 3 mm, D = 0.1 and different Re = 50, 100 and 500

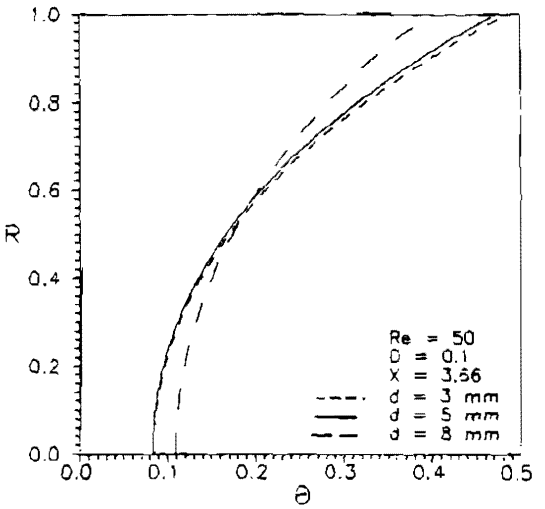

Fig. 13 Temperature distribution at X_e = 3.66 for D = 0.1, Re = 50 and different sphere diameters d = 3, 5 and 8 mm

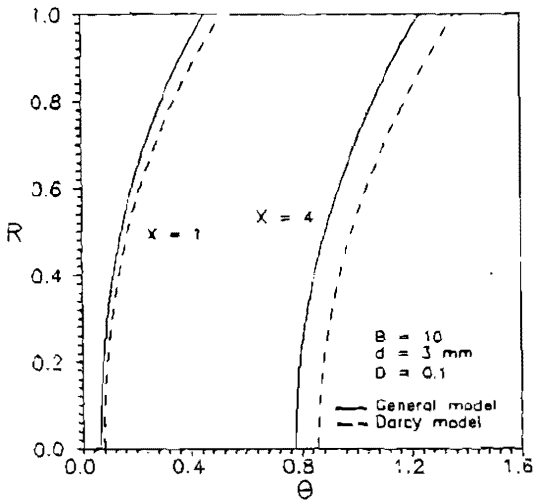

Fig. 14 Temperature distribution at two locations X = 1 and 4 for d = 3 mm, D = 0.1 and B = 10^6 for both general and Darcy flow models

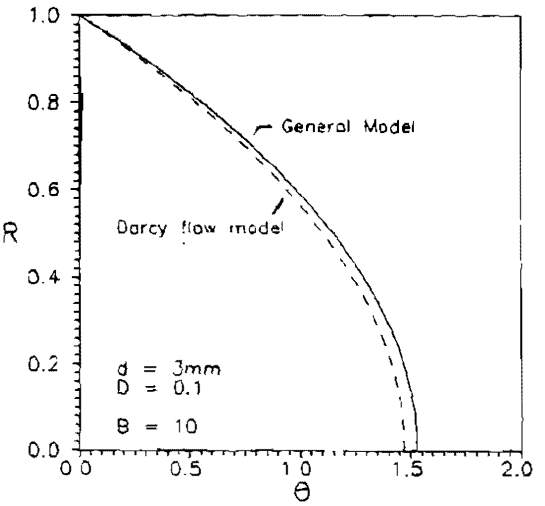

Fig. 15 The mixed mean temperature variation in the fully developed region for d = 3 mm, D = 0.1 and B = 10^6 for both general and Darcy flow models

the flow. This is because of the increase of the channeling effect in the boundary layer and the more fluid flowing in it than that flowing in the core [25].

The temperature variations in two sections in the developing and fully developed regions where X=1 and 4 are shown in Fig. 14, while Fig. 15 presents the invariant mixed mean temperature variation θ_m in the fully developed region for d = 3 mm, D = 0.1 and B=10^6. In the same figures, the temperature and mixed mean temperature variation obtained based on Darcy flow model are reported. Since the Darcy flow model does not satisfy the no-slip condition and since it assumes constant porosity (ε_e), it yields a uniform slug velocity profile. Therefore, the general flow model yields a more effective thermal communication between the fluid and the solid boundary compared with the Darcy model.

5. Conclusions

Forced convection heat flow through a circular pipe filled with saturated porous media and exposed to a constant heat flux has been numerically simulated. Both the energy equation and the generalized form momentum equation including the non-Darcian effects such as the variable porosity, flow inertia, and viscous friction are considered, and the finite difference method technique is used. The effect of the system parameters d, D, B and Re on the entrance length, temperature profiles and heat transfer characteristics were studied. Also the effects of the non-Darcian terms on the temperature and Nusselt number is examined. The present conclusions wereobtained:

- The entrance length increases linearly in the logarithmic scale with the nondimensional pressure gradient B or the sphere-diameter-to channel radius ratio D. Also, the entrance length increases with the bead diameter d for constant pressure drop.
- The thermal entrance length X_e increases linearly with Reynolds number, i.e. for constant Reynolds number it does not depend on either d, or D or B and the direct dependence on Re gives the same correlation that obtained for the pure fluid flow case:

$$X_e = 0.1\ Re$$

- Taking into consideration the non-Darcian effects, a noticeable increase of the value of Nu was found in both the entry and fully developed regions. In this case, the value of Nu in the fully developed region is approximately 21 percent higher than the value predicted by the Darcy model.
- Due to the channeling effects near the wall, steeper temperature gradients at the wall exist. With the increase of the bead diameter d the channeling effects lead also to more fluid flowing in the boundary layer than that flowing in the core which yields lower nondimensional temperature θ near the boundary, and higher one in the core of the flow.

- For constant d and D, the increase of Re, i.e. faster flow decreases the nondimensional temperature θ (the difference between the local temperature and the inlet temperature) and leads to thinner thermal boundary layer which yields smaller temperature difference between the boundary and core flows.
- The general flow model yields a more effective thermal communication between the fluid and the solid boundary compared with the Darcy model which assumes uniform slug velocity profile.

6. Nomenclature

A	Forschheimer inertia coefficient of the porous medium, equation 2
b, c	constants, equation 5
B	nondimensional pressure gradient , equation 7
C_1	dimensionless coefficients, equation 7
d	sphere diameter, mm
D	dimensionless sphere diameter = d/r_o
Nu	Nusselt number, equation 8
P	pressure, Pa
q_w	the mean wall heat flux.
r	radial coordinate
r_o	pipe radius
R	dimensionless radial coordinate
Re	Reynolds number based on the tube diameter = $2\, u_m.r_o/\upsilon$
T	temperature, K
T_{in}	temperature at the inlet section $x = x_{in}$
T_m	average temperature, equation 8
T_w	wall temperature
u	field velocities in the x direction, m/s
u_m	Local averaged fluid velocity including the solid and fluid regions
U	non-dimensional field velocity in the X direction
x	axial coordinate
x_{in}	channel inlet axial distance
X	dimensionless distances in the x axis = $(x - x_{in}) / (r_o.Pr)$
X_e	the thermal entry length
α	effective thermal diffusivity of the porous medium, m^2/s
γ	permeability of the porous layer, equation 2, m^2
Γ	dimensionless coefficients, equation 7
ε	porosity of the porous medium
ε_e	free-stream porosity
θ	non-dimensional temperature = $(T - T_{in}) / (q_w \,.\, r_o / \alpha_e)$
θ_m	invariant mixed mean temperature = $(T_w - T) / (T_w - T_m)$
υ	kinematic viscosity of the fluid, m^2/s
ρ	fluid density, kg/m^3

7. References

1. Combarnous, M. A., and Boris, S. A., "Hydrothermal convection in saturated porous media," Advances in Hydroscience, Vol. 10, pp. 231-307, 1975
2. Catton, I., " Natural convection heat transfer in porous media," Natural convection: fundamentals and applications, Hemisphere, New York. 1985.
3. El Kady, M.," Numerical study of natural convection in a rectangular porous medium with vertical temperature gradient," Mansoura Engineering Journal (MEJ), Vol. 15, No. 1, pp. M72-M87, June 1990.
4. Vafia, K., and Tien, C. L., "Boundary and Inertia Effects on Flow and Heat Transfer in Porous Media," Int. J. Heat Mass Transfer, Vol. 24, pp. 195-203, 1981.
5. Poulikakos, D., and Bejan, A., "The departure from Darcy flow in natural convection in vertical porous layer," Physics of fluids, Vol. 28, pp. 3477-3484, 1985.
6. Kladias, N., and Prasad, V., "Natural convection in horizontal porous layers: effect of Darcy and Prandtle numbers," ASME Journal of Heat Transfer, Vol. 111, pp. 927-935, 1989.
7. Lauriat, G. and Prasad, V., "Natural convection in a vertical porous cavity: a numerical study for Brinkman-extended Darcy formulation", Trans. of the ASME, Vol 109, pp. 688-696, 1987.
8. Ettefagh, J., Vafia, K., and Kim, S., "Non-Darcian effects in open ended cavities filled with a porous medium," ASME J. of Heat Transfer, Vol. 113, pp. 747-762, 1991.
9. Koh, J. C. Y., and Colony, R. "Analysis of cooling effectiveness for porous material in cooling passage," ASME , Journal of Heat Transfer, Vol. 96, pp. 324-330, 1974.
10. Kaviany, M., "Laminar Flow Through a Porous Channel Bounded by Isothermal Parallel Plates," Int. J. of Heat and Mass Transfer, Vol. 28, pp. 851-858, 1985.
11. Poulikakos, D., and Renken, K., "Forced Convection in a Channel Filled With Porous Medium, Including the Effects of Flow Inertia, variable Porosity, and Brinkman Friction," ASME, Journal of Heat Transfer, Vol. 109, pp. 880-888, 1987.
12. Renken, K., and Poulikakos, D., "Experiments on forced convection from a horizontal heated plate in a packed bed of glass spheres," ASME Journal of Heat Transfer, Vol. 111, pp. 59-65, 1989.
13. El Kady, M., "Forced Convection Heat Transfer and Flow in an Annular Porous Medium in the Non-Darcian Effects" Mansoura Engineering Journal (MEJ), Vol. 19, No. 3, pp. M9- M26, September 1994.
14. Cheng, P., Hsu, C. T., and Chowdhury, A., "Forced Convection in the Entrance Region of a Packed Channel With Asymmetric Heating," ASME Journal of Heat Transfer, Vol. 110, pp. 946-954, 1988.
15. Wang, B. and Du, J., "Forced convective heat transfer in a vertical annulus filled with porous media" Int. J. of Heat and Mass Transfer, Vol. 36, No. 17, pp. 4207-4213, 1993

16. Amiri, A. and Vafia, K., "Analysis of dispersion effects and non-thermal equilibrium, non-Darcian, variable porosity incompressible flow through porous media" Int. J. of Heat and Mass Transfer, Vol. 37, No. 6, pp. 939-954, 1994
17. Kamiuto, K., and Saitoh, S., "Fully developed forced-convection in heat transfer in cylindrical packed beds with constant wall temperatures," JSME International Journal, series B, Vol. 37, No. 3., pp. 554-559, 1994.
18. Benenati, R. F., and Brosilow, C. B., "Void fraction distribution in Packed Beds," AICHE J., Vol. 8, pp. 359-361, 1962.
19. Vafia, K., Alkire, R. L., and Tien, C. L., " An Experimental Investigation of Heat Transfer in Variable Porosity Media," ASME Journal of Heat Transfer, Vol. 107, pp. 642-647, 1985.
20. Muralidhar, K., and Kulacki, F. A.," Non-Darcy Natural Convection in a Saturated Horizontal Porous Annulus," ASME Heat Transfer Division, HTD Vol. 56 "Natural Convection in Porous Media", pp. 23-31, 1987
21. Chandrasekhara, B. C., and Vortmeyer, D., "Flow Model for Velocity Distribution in Fixed Porous Beds Under Isothermal Conditions," Th.. Fluid Dynamics, Vol. 12, pp. 105-111, 1979.
22. Patankar, S., "Numerical Heat Transfer and Fluid Flow" Mc Graw Hill, New York, 1980.
23. Hirsch, C., " Numerical Computation of Internal and External Flows, Vol. 1: Fundamentals of Numerical Discretization" John Wiley & Sons , 1991.
24. Incropera, F. P., and De Witt, D. P., "Fundamentals of Heat and Mass Transfer" John Willey & Sons, New York, 1990.
25. El Kady, M., Rabie, L., Tolba, M., "Flow in a circular pipe filled with porous medium in the non-Darcian effects," To be Published
26. Kays, W. M., and Crawford, M. E. "Convective Heat and Mass Transfer" Mc Graw Hill, New York, 1980.
27. Petukhov B. C., "Heat transfer and hydraulic resistance in laminar flow of liquid in circular tubes.," Book, M. Energia, 1967.